Int J Appl Earth Obs Geoinformation 74 (2019) 65–77

Contents lists available at ScienceDirect

Int J Appl Earth Obs Geoinformation

journal homepage: www.elsevier.com/locate/jag

Mapping forest aboveground biomass in the reforested Buffelsdraai landfill site using texture combinations computed from SPOT-6 pan-sharpened imagery

Sizwe Thamsanqa Hlatshwayo*, Onisimo Mutanga, Romano T. Lottering, Zolo Kiala, Riyad Ismail

Discipline of Geography, School of Agricultural, Earth and Environmental Sciences, University of KwaZulu-Natal, P/Bag X01, Scottsville, Pietermaritzburg 3209, South Africa

ARTICLE INFO

Keywords:
SPOT-6 imagery
Reforestation
Biomass estimation
Image processing techniques
Texture combinations

ABSTRACT

Developing models for estimating aboveground biomass (AGB) in naturally growing forests is critical for climate change modelling. AGB models developed using satellite imagery varies with study area, depending on the complexity of vegetation and landscape structure, which affects the upwelling radiance. We assessed the potential of SPOT-6 imagery in predicting AGB of trees planted at different time periods, using image texture combinations. Image texture variables were computed from the SPOT6 pan-sharpened image data, which is characterised by a 1.5 m spatial resolution. In addition, we incorporated the minimal variance technique to select the optimum window sizes that best captures AGB variation in our study area. The results showed that image texture was able to detect AGB for both mature and young trees, however, models detecting mature trees were more superior, with accuracies of R^2 = 0.70 and 0.25 for 2009–2011 and 2011–2013 plantation phases, respectively. In addition, our results showed that the three band texture ratios yielded the highest accuracy (R^2 = 0.88 and RMSE = 54.54 kg m^{-2}) compared to two texture (R^2 = 0.85 and RMSE = 60.65 kg m^{-2}) and single texture band combinations (R^2 = 0.64 and RMSE = 94.13 kg m^{-2}). A frequency analysis was also run to determine which bands appeared more frequently in the selected texture band models. The frequency analysis revealed that both the red and green bands appeared more frequently on the selected texture band variables, indicating that they were more sensitive to the variation of AGB in our study area. The results showed high variation in AGB within the Buffelsdraai reforestation site, especially due to varying tree plantation phases as well as topography. In essence, the study demonstrated the possibility of image texture combinations computed from the SPOT-6 image in estimating AGB.

1. Introduction

The estimation of forest above-ground biomass (AGB) distribution across a landscape provides invaluable information for ecological modelling (Dube and Mutanga, 2015a). This enables ecologists to understand the primary productive capacity of the landscape (Gower et al., 1996). Forests play a significant role in carbon cycling as they are responsible for carbon sequestration (Pan et al., 2011; Bastin et al., 2014; Sousa et al., 2015). Therefore, an understanding of forest AGB plays a critical role in climate change modelling and carbon accounting. The utility of forest AGB models for carbon estimations stems from the fact that half of the overall forest AGB is made up of carbon (Nowak and Crane, 2002). Hence, it is important to establish accurate and timely methods of computing forest AGB in natural forests. Conventional methods (such as tree harvesting and measurements of tree height and diameter) for estimating AGB have proven to be subjective, time-consuming, costly or spatially restrictive. Conversely, the combination of remote sensing approaches with field based methods of estimating AGB have proven to be objective, inexpensive or spatially explicit (Sarker and Nichol, 2011; Lottering and Mutanga, 2012; Barbosa et al., 2014; Bastin et al., 2014; Dube et al., 2014; Dube and Mutanga, 2015a).

The advent of optical remote sensing has made it possible to provide estimates of forest AGB that are timely, reasonably accurate and allow for repetitive coverage (Mather and Koch, 2011; Lottering and Mutanga, 2012; Dube et al., 2014). Previous studies focusing on remote sensing of forest AGB have primarily used spectral reflectance of individual bands and vegetation indices with a reasonable degree of accuracy, however with some limitations (Anderson et al., 1993; Dube et al., 2014; Dube and Mutanga, 2015a). For example, studies have indicated that the relationship between forest AGB and spectral

* Corresponding author.
E-mail address: 210511840@ukzn.ac.za (S.T. Hlatshwayo).

https://doi.org/10.1016/j.jag.2018.09.005
Received 31 October 2017; Received in revised form 5 July 2018; Accepted 4 September 2018
Available online 15 September 2018

vegetation indices is negatively affected by rapid vegetation growth rates and canopy shadow (Dengsheng Lu et al., 2002; Dengsheng Lu et al., 2005; Mather and Koch, 2011). As a result, several studies have geared towards the use of image texture analysis, which focuses more on the spatial distribution of grey tone levels within an image (Lu, 2005; Castillo-Santiago et al., 2010; Eckert, 2012).

Texture analysis attempts to compute the degree of image tone variation in high spatial resolution imagery, using statistical parameters to measure the spatial distribution of grey-tones within pixels falling in a particular window size (Wulder et al., 1998). In essence, image texture measures the local variance of grey-tone and is therefore largely dependent on scale (Haralick et al., 1973). The local variance of grey tone in forested areas is a function of changes in species type, the level of crown closure, and stem density (Franklin et al., 2001). Studies have confirmed that texture analyses are capable of improving forest AGB prediction when compared to spectral vegetation indices (Dengsheng Lu and Batistella, 2005; Eckert, 2012). For example, Lu (2005) concluded that raw texture bands outcompeted raw spectral bands in estimating forest biomass. Similarly, Eckert (2012) improved the overall forest AGB estimation using texture bands when compared to raw spectral bands.

The high performance of image texture in predicting forest AGB is attributed to its ability to simplify the forest canopy structure by smoothing the canopy surfaces using statistical texture variables (Wulder et al., 1998; Franklin et al., 2001). However, research has proven that raw texture bands are incapable of eliminating topographic effects on reflected radiance and errors associated with sensor angle and radiance from sunlight (Sarker and Nichol, 2011). Therefore, studies have recently made new avenues in forest AGB estimation by introducing texture band combinations. The use of texture band combinations has achieved a high degree of success in estimating forest AGB, especially when compared to raw texture bands and vegetation indices (Nichol and Sarker, 2011; Sarker and Nichol, 2011; Dube and Mutanga, 2015b). The current study extends the work of Nichol and Sarker (2011); Sarker and Nichol (2011); Dube and Mutanga (2015b), by introducing a new three band texture combination method. This novel method combines the strengths of image texture and band ratios, thus could potentially improve their ability to predict forest AGB. According to Wang et al. (2012) three band combinations contain a large amount of information that has a potential to overcome saturation that is common in two band combinations. Studies have found higher accuracies in mapping vegetation features using three band ratios as oppose to two band ratios (Huete et al., 2002; Gitelson and Gritz, 2003; Verrelst et al., 2015). Therefore, in this study we tested this theory by comparing the accuracy of three band texture ratios against the commonly used two band texture ratios and raw texture bands computed from SPOT-6 pan-sharpened imagery, using random forest (RF) regression and multiple linear regression (MLR). Since texture is largely dependent on scale, we used the minimum variance technique to establish optimum moving windows to detect forest AGB at various stages of succession. Finally, we compared the capability of the SPOT-6 pan-sharpened image to predict AGB of trees planted at different stages of succession.

2. Methods and material

2.1. Study area

This study was conducted in the Buffelsdraai Landfill Site Community Reforestation Project, which is located roughly 25 km North of Durban in KwaZulu-Natal, South Africa (see Fig. 1). The Reforestation project is approximately 520.6 km^2 in size and is situated along the buffer zone of the Buffeldraai landfill site, which is owned by the EThekwini Municipality. The topography of the area is highly undulating with steep hills ranging from 200 m to 325 m above sea level. According to Mucina and Rutherford (2006), the area is located along the KwaZulu-Natal Coastal Belt mainly composed of grassland, which is listed as endangered in the recent vegetation map of South Africa due to fragmentation. The area is predominantly used as a landfill site, and the buffer-zone was previously used for sugarcane, and communal cattle grazing before it was reforested. Over 50 indigenous tree species have been planted in this area from 2009 to 2015 at various stages (i.e. 2009–2010, 2010–2011, 2011–2012, 2012–2013, 2013–2014 and 2014–2015). Summer rainfall dominates this area as it falls along the Indian Ocean, which experiences high annual rainfall of approximately 766 mm/year. The midday average temperature is 22.2 °C and 27.5 °C in winter and summer, respectively. The geology of the area is dominated by the Dwyka Tillite. The poorly drained Glenrosa soil form dominates the study area with Shortlands and Swartland soil forms occupying the majority of the remaining area.

2.2. Image acquisition and pre-processing

The SPOT-6 pan-sharpened image was used due to its high spatial resolution of 1.5 m. This image consists of four bands ranging from 0.450-0.890 μm (see Table 1), covering the visible and near infrared region of the spectrum. The image was freely acquired from the South African Space Agency (SANSA) on the 11th of April 2015, at 07:44:38am. The images were Ortho-projected courtesy of SANSA.

The images were mosaicked using ERDAS imagine mosaic-pro tool for further processing. The SPOT-6 image was then atmospherically corrected to the top of the canopy reflectance using the algorithm Fast Line-of-Sight Atmospheric Spectral Hypercubes in ENVI 4.7 software (FLAASH). In order to assess the full potential of the 1.5 m spatial resolution of the SPOT-6 panchromatic image, the image was pan-sharpened using the Intensity-Hue-Saturation (IHS) method. The IHS method was chosen based on the findings of Strait et al. (2008) who discovered that this method preserves the spectral resolution of remotely sensed imagery and improves the spatial resolution of the image. This makes the pan-sharpened image suitable for spatial analysis such as texture indices, which are scale dependent.

2.3. Field measurements

The purpose of this study was to establish a monitoring system for AGB in re-afforested ecosystems at different temporal scales. Therefore, the site was divided into different plantation phases. It is important to take into consideration the complex vegetation structure that exists within the study site, which is composed of trees and grasses that grow at proportional heights. For the purpose of this study, only the plantation phases that were 3 years and older were considered, ranging from 2009 to 2010, 2010–2011 to 2011–2012. These age groups had enough canopy cover to minimise soil background reflectance. Field data collection was conducted in September 2015; the same year the image was acquired.

A set of ninety 35 X 35 m random plots were generated in ArcGIS 10.3, covering the Buffelsdraai planted sites. These random plots were then located infield using a Trimble Geo 7x GPS with sub-meter accuracy. In each plot, all the trees were measured for diameter at ankle height and total tree height using a caliper and ranging rod, respectively.

2.4. Field biomass calculations

Dry biomass was calculated using the following general allometric equation developed by Chave et al. (2005), for tropical dry forest stands:

$$AGB = 0.112 \times (\rho D^2 H)^{0.916} \quad (1)$$

Where AGB is total above-ground biomass, ρ is wood density, D is diameter at ground level and H is total tree height. Wood density (ρ) was derived from published wood density values that were derived

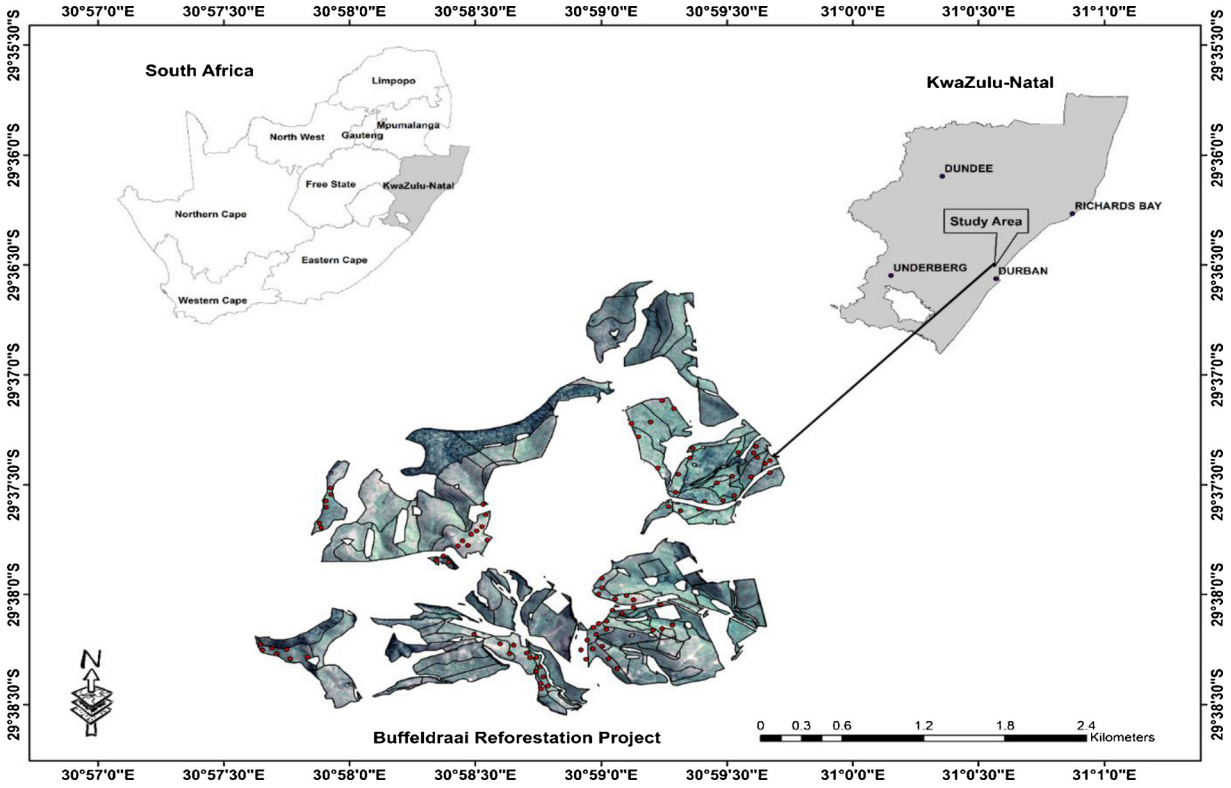

Fig. 1. Location of study site and the SPOT-6 image of the Buffelsdraai Reforested site.

Table 1
The spectral bands and spatial resolutions of the SPOT-6 pan-sharpened image.

Band Number	Spectral Color	Range (μm)	Spatial Resolution (m)
Band 1	Blue	0.450-0.520	1.5
Band 2	Green	0.530-0.590	1.5
Band 3	Red	0.625-0.695	1.5
Band 4	Near Infrared	0.760-0.890	1.5

Table 2
The selected representative classes for optimum window size selection.

Succession Period	Biomass (kg m^{-2})	Number of Plots
2009-2011	0-220	14
	221-440	12
	441-680	21
2011-2013	0-115	20
	116-230	18
	231-360	4

under similar bioclimatic zones to our study area. The AGB for all tree species within a plot were determined and subsequently averaged to obtain a representative value per plot.

2.5. Optimum window selection

Since image texture is a function of spatial resolution of an image, we applied the method proposed by Marceau et al. (1994) to select the optimum window size that best captures forest AGB at various stages of development (i.e. 2009–2011 and 2011–2012). Herein, the variance is calculated for each window size to determine the level of pixel value variation within that particular window (Peerbhay et al., 2016). This method involves firstly, the selection of classes that best represent the geographic entity (forest AGB) under investigation, secondly the re-sampling of the SPOT-6 pan-sharpened image to produce the images with varying window size, and thirdly the calculation of variance for each window size using the selected representative classes.

2.5.1. Characterising the representative classes for forest AGB levels for each succession stage

This study used, age of trees (i.e. 2009–2011 and 2011–2012) and forest AGB as a criterion for determining the optimum window size for forest AGB estimation. Herein, sampled plots that best represent varying forest AGB were identified. Table 2 shows the results for the representative classes used to characterise varying levels of forest AGB. Based on field measurements the older trees had higher forest AGB cover compared to younger trees.

2.5.2. Resampling the SPOT-6 pan-sharpened image

This step involves the resampling of the SPOT-6 pan-sharpened image prior to atmospheric correction using odd size windows (*nxn*). Varying window sizes were used in this study (i.e. 3 × 3, 5 × 5, 7 × 7, 9 × 9, 11 × 11, 13 × 13, 15 × 15, and 17 × 17). The image resampling procedure was carried out using the nearest neighbor resampling technique in ArcGIS 10.3. This resulted in 8 images for each spectral band with varying spatial resolutions. Subsequently, the DN values of the pixels were extracted using the zonal statistic tool in ArcGIS 10.3. The utility of this method to spatially resample remotely sensed images was recommended by Franklin et al. (1995), with an assumption that pixel values represent an average DN value of a particular area on the ground.

2.5.3. Minimum variance calculation

This step involves the calculation of the minimum variance of all the window sizes for each individual band. This method assumes that a smaller window size only captures a small component of the geographic entity (Marceau et al., 1994). In this case, variance increases as a result of intra forest AGB variation. Therefore, if the window size is larger than the geographic entity under study, more geographic entities are captured by the window size, as a result variance increases. The

Table 3
Definition and equations of GLOM texture measures.

Parameter	Formula	Description
Mean	$Mean = \frac{\sum_k x_k}{k}$	Computes the average values of spectral reflectance at each window (Lottering and Mutanga, 2012).
Data range	$max\{X\}-min\{X\}$	Calculates the difference between the lowest and highest pixel values (St-Louis et al., 2006)
Entropy	$\sum_{i=0}^{M-1} p(i)log_2[p(i)]$	This is a measure of the degree of histogram uniformity (Materka and Strzelecki, 1998).
Skewness	$\mu_{3=}\sigma^{-3}\sum_{i=0}^{M-1}(i-\mu)^3 p(i)$	Measures the level of histogram asymmetry around the mean (Materka and Strzelecki, 1998).
Variance	$\frac{\sum(xij-M)^2}{m-1}$	Variance determines the variability of the pixel values within a moving window (Materka and Strzelecki, 1998)

optimum window size therefore is attained when the geographic entity is homogenous, this is indicated by minimum variance (Lottering and Mutanga, 2016). Studies have confirmed that the selection of optimum window size is vital for improving vegetation detection and the predictive performance of the models (Ismail et al., 2008; Lottering and Mutanga, 2016; Peerbhay et al., 2016). The variance of pixel values for all the bands of the pan-sharpened image (n = 4) was determined using Eqs. (2) and (3). Since the variance for band 4 among the different window sizes was similar, only band 1, 2 and 3 were used to select the optimum window size.

$$Variance = \frac{\sum (x_{ij}-M)^2}{n-1} \quad (2)$$

$$Mean = \frac{\sum x_{ij}}{n} \quad (3)$$

Where M is the mean of the digital numbers (DN) within a moving window, x_{ij} denotes the DN values for the pixels and n is the number of pixels within a moving window.

The variance of each window size was plotted as a function of window size, wherein the initial trough of the variance for each band was regarded as the optimum window size.

2.6. Image texture analysis

Texture parameters are commonly used to measure the spatial distribution of image tone variance (Moskal and Franklin, 2001), which can be used to estimate forest AGB. Herein image tone refers to the variation of grey scales of resolution cells in an image (Mather and Koch, 2011). Variation in image tone can result from changes in stem density, species type, or crown closure (Franklin et al., 2001). In this study, two sets of texture measures were utilised namely: co-occurrence and occurrence measures. With the use of grey-level occurrence measures (GLOM), texture is calculated using the pixel intensities of the histogram within a processing window. This method does not consider the spatial dependency of pixels (St-Louis et al., 2006). The GLOM consists of five filters used to calculate texture, namely: mean, data range, variance, skewness and entropy. For the description of the GLOM filters, refer to Table 3.

On the other hand, the grey-level co-occurrence matrix (GLCM) uses a spatial dependent grey tone matrix to compute texture (Haralick et al., 1973). The GLCM filters include, variance, mean, contrast, homogeneity, correlation, entropy, dissimilarity and second moment. Table 4 provides a brief description of GLCM filters.

Both the GLOM and GLCM filters utilise a specified angle and direction to compute texture measures. However, the purpose of this study is to establish the appropriate filter and window size to extract texture for forest AGB estimation, thus one angle of 45° was used. The basis of choosing the 45° angle was founded upon the fact that it has minimal effect on coefficient of determination (R^2) (Lottering and Mutanga, 2012). The window sizes used to compute texture images were selected based on the method explained above proposed by Marceau et al. (1994). Texture indices were derived from the SPOT-6 pan-sharpened image. The SPOT-6 pan-sharpened texture indices were processed in three steps:

Step1: The single texture parameters of the SPOT-6 pan-sharpened image were tested in predicting forest AGB using a RF and MLR.

Step2: The pan-sharpened image was then processed further using two band texture parameters and their accuracy in predicting forest AGB was assessed in RF and MLR. All possible two band texture combinations were computed using Eqs. (4) to (6):

$$\frac{B1}{B2} \quad (4)$$

$$B1-B2 \quad (5)$$

$$\frac{B1-B2}{B1+B2} \quad (6)$$

Where B1 and B2 are texture parameters.

Step3: The pan-sharpened image was then processed further by combining the bands using three texture parameters and their accuracy in predicting forest AGB was assessed using a RF and MLR. All possible three band texture combinations were computed using Eq. (7):

$$\frac{B1}{B2 \times B3} \quad (7)$$

Where B1, B2 and B3 are texture parameter.

2.7. Extracting texture parameters

The field data containing forest AGB plots and their GPS coordinates

Table 4
Definitions and equations of GLCM texture measures.

Parameter	Formula	Description
Contrast	$\sum_{i,j=0}^{M-1} P_{i,j}(i-j)^2$	Calculates the level of local variation within a window (Yuan et al., 1991)
Correlation	$\sum_{i,j=0}^{M-1} P_{i,j}\left[\frac{(i-\mu_i)(i-\mu_j}{(\sigma_i^2)(\sigma_j^2)}\right]$	Measures the grey-level linear-dependency within an image (Kayitakire et al., 2006)
Dissimilarity	$\sum_{i,j=0}^{M-1} P_{i,j}\ \lvert i-j\rvert$	Is a measure of the local variation (Rubner et al., 2001).
Homogeneity	$\sum_{i,j=0}^{M-1} \frac{P_{i,j}}{1+(i-j)^2}$	Measures the smoothness of image texture (Tuttle et al., 2006)
Mean	$\mu_i = \sum_{i,j=0}^{M-1} i(P_{i,j})$ $\mu_j = \sum_{i,j=0}^{M-1} j(P_{i,j})$	Average grey-level in the small neighborhood (Materka and Strzelecki, 1998)
Second Moment	$\sum_{i,j=0}^{M-1} P_{i,j}{}^2$	Second moment is an indicator of local homogeneity (Yuan et al., 1991)
Variance	$\sigma_i^2 = \sum_{i,j=0}^{M-1} P_{i,j}(i-\mu)^2$ $\sigma_j^2 = \sum_{i,j=0}^{M-1} P_{i,j}(i-\mu_j)^2$	Variability of the spectral response of pixels (Materka and Strzelecki, 1998).
Entropy	$\sum_{i,j=0}^{M-1} P_{i,j}(-lnP_{i,j})$	A statistical measure of uncertainty (Yuan et al., 1991)

Where $P(i,j)$ is the normalized co-occurrence matrix where the sum of ($i,j = 0, M-1$)($P(i,j)$) = 1.

were used to establish a point map. The point map was superimposed upon the texture index images to establish a region of interest (ROI) map using the central points of the GPS coordinates per plot. The texture values were extracted using the zonal statistics tool in ArcMap 10.3. The collected texture dataset was then input into a MLR to generate prediction biomass models.

2.8. Statistical analysis

The relationship between natural forests aboveground biomass and image texture variables was modelled using random forest (RF) algorithm and multiple linear regression (MLR). Random forest (RF) is a collection of learning techniques, which he developed to advance the classification and regression trees (CART) method by compiling a large set of decision trees (Breiman, 2001). The advantage of using the RF algorithm is that, it is able to optimize the classification and regression trees (ntree) method by combining a large set of decision trees (Breiman, 2001). Each of these trees are constructed using a deterministic algorithm, whereby a random set of variables are selected and a random sample from the training dataset is selected (James et al., 2013). In addition the random forest algorithm is able to improve model performance by optimizing: mtry the number of different predictors tested at node (the default is1/3) and ntree the number of trees grown based on bootstrapped of observation (Mutanga et al., 2012). The machine learning technique was implemented using Python language statistical interface. In python the random search function was used to optimize the ntree and mtry parameters, the function selected the best combination of parameters (i.e. ntree and mtry) based on the lowest root mean square error (RMSE) of calibration dataset. The ntree values were tested in increments of 500 to 2500 and the mtry values were tested in increments of 1 to 5, both based on single value interval (Dube et al., 2014). The results from the RF algorithm were then compared to the MLR to assess its performance.

2.9. Relationship between texture indices and AGB

The field data was tested for normality of distribution using the Shapiro-Wilk test to assess whether there were any normality violations. Normality tests are a prerequisite prior to running parametric statistical tests as they assume that the data follows a normal distribution (Mutanga and Skidmore, 2004). The relationship between forest AGB dataset and image texture parameters were tested using Pearson's correlation. The input texture parameters undergone sequential forward selection prior to Pearson's correlation test, where only significant texture indices were selected. The texture indices selected were then input into the RF and MLR to develop forest AGB models.

2.10. Model validation

To evaluate model performance, the dataset (n = 90) was split into 70% training (n = 63) and 30% test (n = 27) dataset and the 10-fold cross validation technique was implemented to robustly test the performance of the algorithms. The training dataset was used to optimize and train the model and the test dataset was used to verify the predictive ability of the model. The performance of each model in estimating biomass was tested using the root mean square error (RMSE), % RMSE and the coefficient of determination (R^2). In the 10-fold cross validation the data (n = 90) was divided equally into groups of 10 (n = 9), one of the groups was reserved for testing (n = 9) the rest of the data was used to train the model. This process was repeated k-fold, in this case 10-fold, an average RMSE and R^2 was then computed from the test dataset to measure the accuracy of the model.

$$RMSE = \sqrt{\frac{SSE^2}{n}} \quad (8)$$

Table 5
Explanatory statistics of the observed above ground biomass (kg m^{-2}).

Period	n	Mean	Std. dev	Min.	Max.	Range
2009-2011	48	335.07	144.65	98.33	670.43	572.09
2011-2013	42	193.03	73.62	39.73	351.83	312.11
Total Data	90	268.79	136.47	39.73	670.43	630.69

$$RMSE\% = \frac{RMSE}{MEAN} \times 100 \quad (9)$$

The SSE notation represents the sum of errors of (measured biomass-predicted biomass) and n represents the number of predictors involved in the model construction. The model with the lowest RMSE and highest R^2 value was set-aside and used to predict forest AGB. The model that yielded the highest performance was then used to construct a forest AGB map for the study site in ArcMap 10.3.

3. Results

3.1. Descriptive statistics

Descriptive statistics of biomass measured in the field for both the plantation phases (i.e. 2009–2011 and 2011–2013) and combined dataset are shown in Table 5. The Shapiro-Wilk test revealed that the dataset was normally distributed ($p < 0.05$); subsequently the data was further analysed using parametric tests. The highest average tree biomass of 335.07 kg m^{-2} was obtained from the 2009–2011 plantation phase and the lowest was observed for the 2011–2013 plantation phase which was 193.03 kg m^{-2}. Furthermore, the 2009–2011 plantation phase contained the highest maximum AGB of 670.43 kg m^{-2} compared to the 2011–2013 plantation phase with a maximum AGB of 351.83 kg m^{-2}. These results show a directly proportional relationship between the time of plantation and forest AGB (i.e. the older the tree, the higher its biomass).

3.2. Window size selection

The graphs illustrating the variance of pixel values of older trees (i.e. 2009–2011) at various window sizes under varying forest AGB content are displayed in Fig. 2. The optimum window size was reached when the geographic entity and the window size are equal, which is indicated by minimal variance. As stated, the optimum window size was indicated by the first trough in the variance. The results in Fig. 2 indicates that for older trees (i.e. 2009–2011) with moderate to high forest AGB, their optimum window size was 7 × 7 and for older trees with low forest AGB, their window size was 5 × 5.

Fig. 3 illustrates results of variance for the younger trees (i.e. 2011–2013) at various window sizes and under varying forest AGB content. The results in Fig. 3 indicates that the optimum window size for younger trees (i.e. 2011–2013) with moderate to high forest AGB was 5 × 5 and for young trees with low forest AGB, their window size was 3 × 3.

Overall, the results indicate that younger trees were best detected using smaller window due to the small amount of their AGB, whereas older trees exhibited homogeneity in spectral variance at slightly higher window sizes in this case 5 × 5 and 7 × 7.

3.3. Correlation analysis

The Pearson's correlation test was conducted to assess the significance of the relationship between band texture ratios and forest AGB. Table 6 shows the relationship between forest AGB and the texture variables that yielded the highest correlation scores. These texture variables were subsequently used in the MLR and RF regression to construct models for predicting forest AGB. The Pearson correlation's

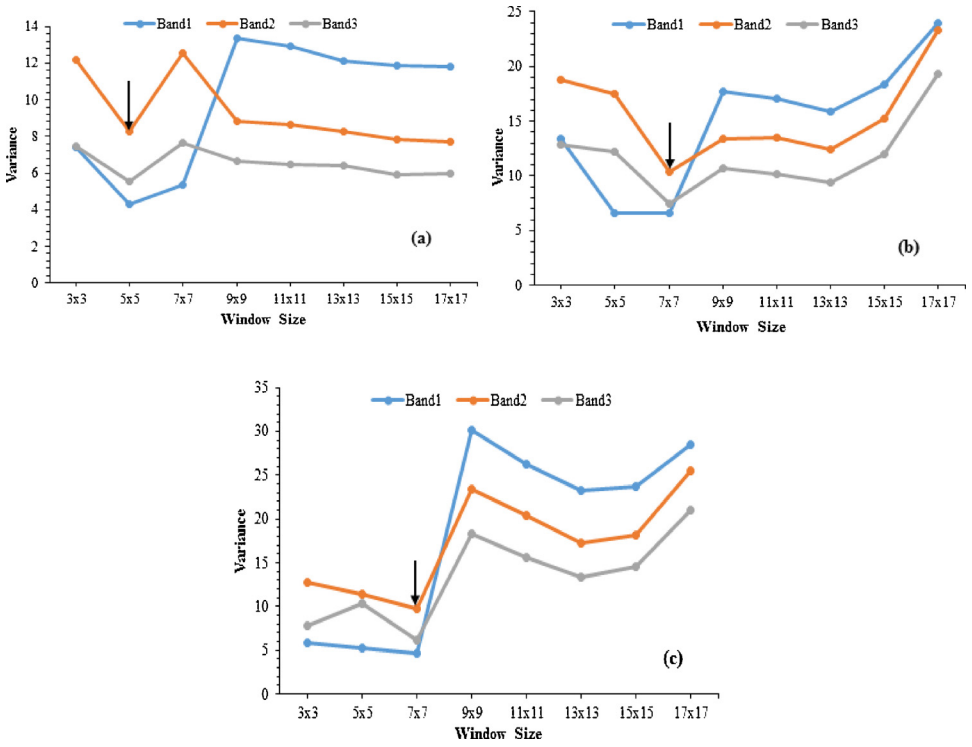

Fig. 2. Optimum window sizes for the 2009–2011 plantation phase selected based on minimal variance of pixel values indicated by black arrows, under varying forest AGB classes. Herein, a, b, and c represent 0–220 (kg m^{-2}), 221–440 (kg m^2) and 441–680 (kg m^{-2}) forest AGB, respectively.

test demonstrated that there is a high agreement between tree AGB and the three band texture combinations. Followed by the two texture band combinations with the Pearson's correlation as high as 0.76. The raw band texture variables yielded the lowest Pearson's correlations with the highest r score of 0.55. Moreover, it is also evident that the selected texture variables were developed mostly using the co-occurrence texture parameters computed from the red band (B3) and the near infrared band (B4).

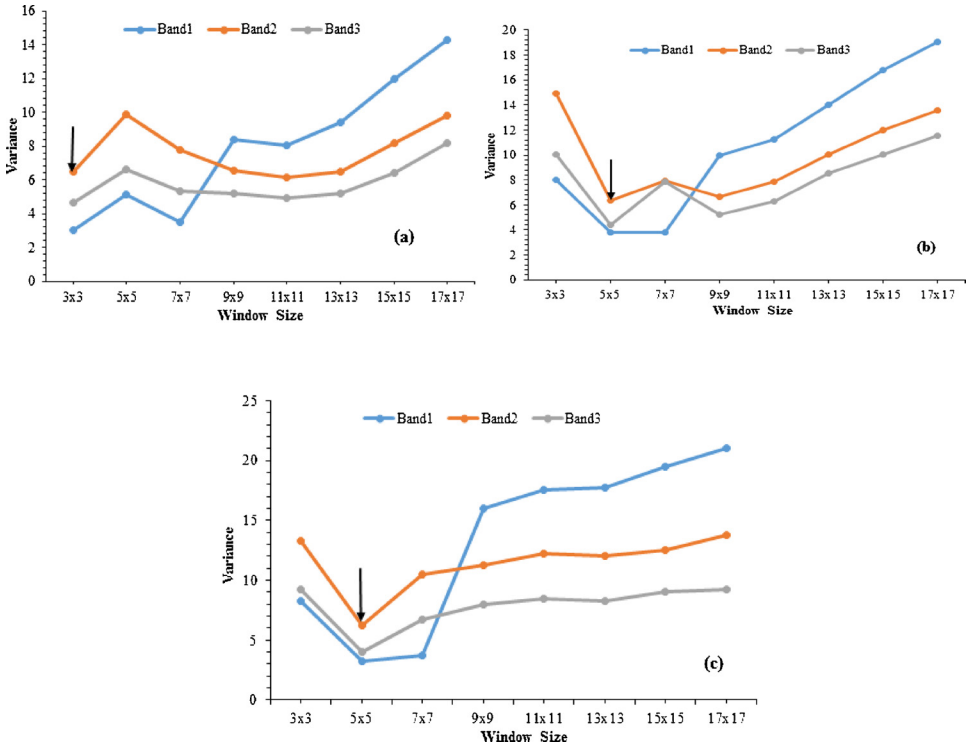

Fig. 3. Optimum window sizes for the 2011–2012 plantation phase selected based on minimal variance of pixel values indicated by black arrows, under varying canopy cover percentage classes. Herein a, b and c represent 0–115 (kg m^{-2}), 116–230 (kg m^{-2}), and 231–360 (kg m^{-2}) percentage canopy cover, respectively.

Table 6
Three band texture combinations for the pan-sharpened image models significant ($p < 0.05$).

Image Processing level	Image texture variable	r
Raw band textures	CN_C_5_B4	0.55
	MN_O_7_B4	0.54
	SM_C_3_B2	0.53
Two band texture ratios	$MN\_C\_3\_B4 - MN\_C\_5\_B2$	0.72
	$\frac{DR\_O\_7\_B3 - SM\_C\_7\_B3}{DR\_O\_7\_B3 + SM\_C\_7\_B3}$	0.74
	$EN\_O\_7\_B3 / SM\_C\_7\_B3$	0.76
Three band texture ratios	$\frac{MN\_C\_3\_B4}{HM\_C\_7\_B2 \times MN\_C\_3\_B3}$	0.82
	$\frac{EN\_O\_7\_B3}{CR\_C\_7\_B3 \times HM\_C\_7\_B4}$	0.80
	$\frac{DR\_O\_7\_B4}{SM\_C\_7\_B3 \times VR\_O\_7\_B2}$	0.79

B1, B2, B3, B4: Band 1, Band 2, Band 3 and Band 4; HM: Homogeneity, EN: Entropy, SM, Second moment, MN: Mean, DR: Data range, CR: Correlation, VR: Variance, CN: Contrast; O: Occurrence, C: Co-occurrence; 3, 5, 7: 3 × 3, 5 × 5 and 7 × 7.

3.4. Predicting AGB of the 2009–2011 and 2011–2012 plantation phases: based on the raw texture bands

A comparative analysis was conducted to assess the accuracy of the SPOT6 pan-sharpened image in predicting biomass of the 2009–2011 and 2011–2013 forest plantation phases. The results in Table 7 shows the predictive performance of the raw band texture for the divided dataset according to the plantation phases mentioned above and the pooled dataset.

The results in Table 7 depicts that the raw texture variables computed from the SPOT6 pan-sharpened image were able to predict forest AGB for the 2009–2011 plantation phase better than the 2011–2013 plantation phase. For instance, an R^2 of 0.86 and 0.70 was obtained for the 2009–2011 plantation phase using the MLR and RF regression respectively. Compared to the 2011–2013 plantation phase which produced an R^2 of 0.23 and 0.25, using the MLR and RF regression respectively, all the results are based on an independent test dataset. In addition, the models for 2011–2013 plantation phases produced the highest RMSE values when compared to the models for the 2009–2011 plantation phases. For example, the RMSE values for the 2011–2013 plantation phase were 55.26 kg m^{-2} (28.63%) and 54.17 kg m^{-2} (28.06%) using MLR and RF regression, respectively. Whilst for the 2009–2011 plantation phase RSME values were 46.19 kg m^{-2} (13.79%) and 81.55 kg m^{-2} (24.34%), using MLR and RF regression, respectively. The combined dataset produced moderate accuracy results, indicating the presence of the low accuracy bearing young trees combined with the high accuracy producing older trees with the highest R^2 of 0.67 and 0.63 for the MLR and RF regression respectively, based on an independent test dataset.

3.5. Variable importance measures

The importance of derived texture variables in predicting forest AGB was measured using the OOB error rate in RF. The RF algorithm explored the contribution of each texture variable in predicting forest AGB and ranked them according to their importance. Table 8 shows the top 20 important texture variables ranked according to the decreasing OOB error rate, which indicates the deterioration of the model performance when each predictor is permutated. The results in Table 8 indicates that the number of texture variables that contributed significantly towards predicting forest AGB was high in raw band textures and decreased when using two and three band texture combinations. Notably, the co-occurrence texture measures appeared more frequently on the high ranking texture variables and band 4 (NIR-band) was frequently selected by the highly important variables (see Table 8).

After ranking the texture variables according to their importance, variable selection was conducted to identify the optimum number of variables for predicting forest AGB. Herein the RMSE of the calibration dataset was used to select the optimum number of variables that yielded the lowest RMSE when predicting forest AGB. The variable selection results in Fig. 4 depicts that for raw band texture eight variables were selected with the lowest RMSEC of 41.52 kg m^{-2} (15.45%) of the mean), for two band texture combinations five variables were selected that produced a RMSEC of 30 kg m^{-2} (11.16%) and for three band texture combinations seven variables were selected that produced an RMSEC of 31.01 kg m^{-2} (11.53%). Generally, the results indicate that the accuracy of all the texture models increased as the least important variables were progressively removed and finally the use of most important variables yielded the lowest RMSEC. The selected texture variables were used to fit the MLR and the RF algorithm in order to predict forest AGB.

3.6. Predictive performance of SPOT6 texture combination models

The purpose of this analysis was to compare the accuracy of raw texture bands against two-band texture combinations and three band texture combinations in predicting forest AGB. Table 9 shows the predictive accuracy results for the texture models. Significantly, high variation in accuracies were obtained between the texture models with R^2 values ranging from 0.29 to 0.93. Generally, the RF algorithm outperformed the MLR as expected with R^2 ranging from 0.53 to 0.93 for RF and 0.29 to 0.85 for MLR.

Most interestingly the three textural processing methods used in this study produced significantly different results using both RF and MLR. The accuracy of texture variables increased from $R^2 = 0.64$, 0.85 to 0.88, and from 0.53, 0.67 to 0.77 using test dataset and 10-fold-cross-validation method of single band texture, two band texture combinations and three band texture combinations, respectively. Fig. 5, illustrates a linear relationship between measured and predicted biomass for all the texture variables. These models were developed using the RF, the graphs display the test dataset and the 10 fold cross-validation.

Fig. 5 shows that the three band texture models produced the highest overall predicted performance with an R^2 of 0.88 and 0.77 compared to both the two band texture ratios ($R^2 = 0.85$ and 0.67) and raw texture bands ($R^2 = 0.64$ and 0.53) based on an independent test dataset and 10 fold cross-validation, respectively. The results showed an improved accuracy in the estimation of forest AGB using band texture ratios. The best

Table 7
Accuracy of raw band texture in predicting forest AGB at different plantation phases.

		2009-2011		2011-2013		Combined dataset	
Texture variable	Dataset	R^2	RMSE (kgm^{-2})	R^2	RMSE (kgm^{-2})	R^2	RMSE (kgm^{-2})
Multiple Linear Regression	Train	0.83	56.37 (16.82%)	0.48	50.93(26.38%)	0.51	91.39(34.00%)
	Test	0.86	46.19 (13.79%)	0.23	55.26(28.63%)	0.67	89.92(33.45%)
	5-FoldCV	0.76	70.04(20.90%)	0.22	80.303(41.60%)	0.29	114.72(42.68%)
Random Forest Regression	Train	0.86	36.68(10.95%)	0.70	27.85(14.43%)	0.79	42.70(15.89%)
	Test	0.70	81.55(24.34%)	0.25	54.17(28.06%)	0.63	94.13(35.02%)
	5-FoldCV	0.73	75.05(22.40%)	0.36	58.09(30.09%)	0.39	105.24(39.15%)

Table 8
Variable importance measurements of texture models in predicting forest AGB using RF. Higher OOB error signifies higher variable importance.

	Raw band textures		Two band textures		Three band texture	
Rank	Variable	OOB Error	Variable	OOB Error	Variable	OOB Error
1	SM_C_3_B2	0.128	$MN\_C\_3\_B4 - MN\_C\_5\_B2$	0.216	$\frac{MN\_C\_3\_B4}{CR\_C\_7\_B2 \times MN\_O\_5\_B2}$	0.222
2	CN_C_5_B4	0.100	$MN\_C\_3\_B4 - MN\_O\_5\_B2$	0.175	$\frac{MN\_C\_3\_B4}{MN\_O\_5\_B2 \times CR\_C\_7\_B2}$	0.209
3	MN_C_3_B4	0.0869	$MN\_O\_5\_B4 / CR\_C\_7\_B3$	0.083	$\frac{MN\_C\_3\_B4}{HM\_C\_7\_B2 \times MN\_C\_3\_B3}$	0.139
4	EN_O_5_B1	0.0761	$MN\_C\_5\_B2 - MN\_C\_3\_B4$	0.081	$\frac{MN\_C\_3\_B4}{MN\_C\_3\_B3 \times HM\_C\_7\_B2}$	0.115
5	MN_C_7_B4	0.0610	$MN\_C\_5\_B2 - MN\_O\_3\_B4$	0.054	$\frac{MN\_O\_5\_B4}{MN\_C\_3\_B3 \times HM\_C\_7\_B2}$	0.0625
6	EN_C_7_B4	0.0527	$MN\_C\_3\_B4 - MN\_O\_3\_B2$	0.049	$\frac{MN\_C\_3\_B4}{MN\_O\_5\_B1 \times CR\_C\_7\_B3}$	0.0615
7	CN_C_7_B4	0.0443	$MN\_C\_3\_B4 / CR\_C\_7\_B3$	0.0363	$\frac{EN\_O\_7\_B3}{CR\_C\_7\_B3 \times HM\_C\_7\_B4}$	0.0523
8	DR_O_5_B4	0.0292	$EN\_O\_7\_B3 / SM\_C\_7\_B3$	0.0279	$\frac{MN\_C\_7\_B4}{MN\_C\_3\_B3 \times HM\_C\_7\_B2}$	0.0238
9	HM_C_5_B4	0.0283	$MN\_O\_3\_B2 - MN\_O\_3\_B4$	0.0230	$\frac{EN\_O\_7\_B3}{HM\_C\_7\_B4 CR\_C\_7\_B3}$	0.0199
10	DS_C_7_B4	0.0273	$MN\_O\_3\_B2 - MN\_C\_5\_B4$	0.0225	$\frac{MN\_O\_5\_B4}{HM\_C\_7\_B2 \times MN\_C\_3\_B3}$	0.0140
11	MN_C_5_B3	0.0267	$\frac{MN\_O\_3\_B1 - DR\_O\_7\_B2}{MN\_O\_3\_B1 + DR\_O\_7\_B2}$	0.0208	$\frac{MN\_C\_3\_B4}{CR\_C\_7\_B3 \times MN\_O\_5\_B1}$	0.0123
12	VR_C_5_B4	0.0242	$EN\_O\_7\_B3 / CR\_C\_7\_B2$	0.0197	$\frac{MN\_C\_7\_B4}{HM\_C\_7\_B2 \times MN\_C\_3\_B3}$	0.0111
13	EN_O_7_B2	0.0206	$MN\_O\_5\_B3 - MN\_C\_3\_B4$	0.0159	$\frac{MN\_O\_5\_B4}{MN\_O\_5\_B1 \times SM\_C\_7\_B3}$	0.0109
14	HM_C_3_B1	0.0204	$\frac{VR\_O\_7\_B2 - MN\_O\_7\_B1}{VR\_O\_7\_B2 + MN\_O\_7\_B1}$	0.0156	$\frac{MN\_O\_5\_B4}{SM\_C\_7\_B3 \times MN\_O\_5\_B1}$	0.0108
15	DR_O_3_B3	0.0202	$MN\_C\_5\_B4 - CR\_C\_7\_B3$	0.0148	$\frac{MN\_O\_7\_B4}{HM\_C\_7\_B2 \times MN\_CO\_3\_B3}$	0.0101
16	SM_C_5_B3	0.0162	$\frac{SM\_C\_7\_B3 - VR\_O\_7\_B2}{SM\_C\_7\_B3 + VR\_O\_7\_B2}$	0.0142	$\frac{MN\_O\_7\_B4}{MN\_C\_3\_B3 \times HM\_C\_7\_B2}$	0.0081
17	MN_C_5_B4	0.0152	$\frac{VR\_O\_7\_B2 - HM\_C\_7\_B4}{VR\_O\_7\_B2 + HM\_C\_7\_B4}$	0.0128	$\frac{MN\_C\_7\_B4}{SM\_C\_7\_B3 \times MN\_O\_5\_B1}$	0.0053
18	DR_O_3_B1	0.0147	$MN\_O\_7\_B4 / CR\_C\_7\_B3$	0.0125	$\frac{MN\_C\_3\_B4}{MN\_O\_5\_B1 \times SM\_C\_7\_B3}$	0.0049
19	MN_O_7_B3	0.0137	$\frac{MN\_O\_7\_B1 - VR\_O\_7\_B2}{MN\_O\_7\_B1 + VR\_O\_7\_B2}$	0.0118	$\frac{MN\_C\_3\_B4}{SM\_C\_7\_B3 \times MN\_O\_5\_B1}$	0.0036
20	MN_O_3_B4	0.0128	$MN\_O\_7\_B4 / SM\_C\_7\_B3$	0.0117	$\frac{MN\_C\_7\_B4}{MN\_O\_5\_B1 \times SM\_C\_7\_B3}$	0.0026

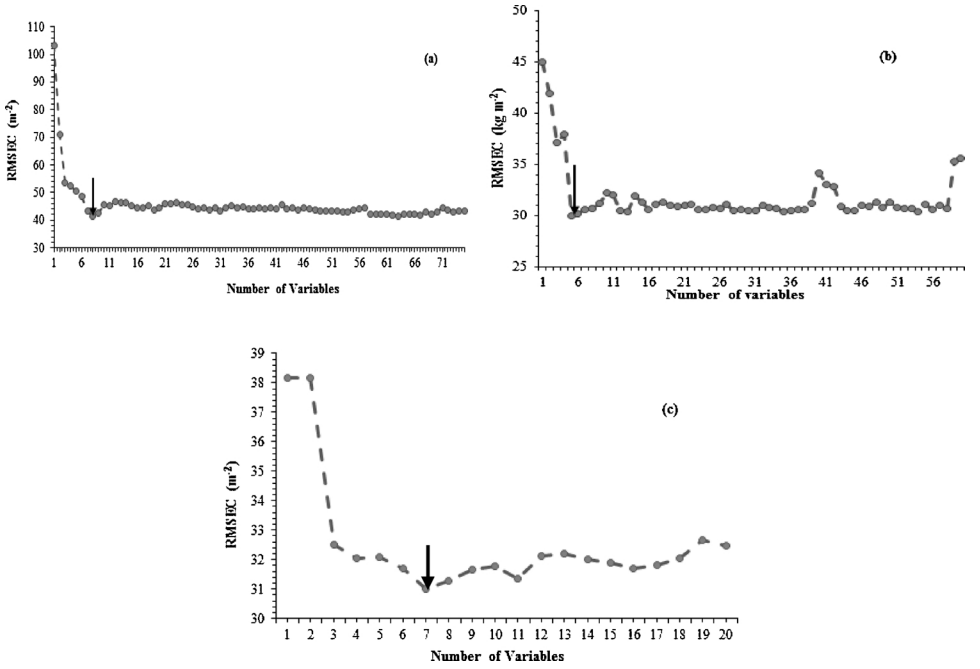

Fig. 4. Selection optimum number of variables (texture) for predicting forest AGB using backward elimination search function.

Table 9
Predictive Performance of the texture models.

				Train dataset		Test Dataset		10-Fold-CV	
Texture variable	Model	mtry	ntree	R^2	RMSE kg m^{-2} (RMSE %)	R^2	RMSE k m^{-2} (RMSE %)	R^2	RMSE kgm^{-2} (RMSE %)
Raw band texture	MLR	–	–	0.51	91.40(34.00%)	0.67	89.92(33.45%)	0.29	114.722(42.68%)
	RF	1	893	0.79	42.70(15.89%)	0.64	94.13(35.02%)	0.53	92.82(34.53%)
two band texture ratio	MLR	–	–	0.67	75.24(27.99%)	0.82	67.09(24.96%)	0.63	82.89(30.84%)
	RF	1	860	0.90	40.20(14.96%)	0.85	60.65(22.56%)	0.67	77.56(28.86%)
three band texture ratio	MLR	–	–	0.76	63.69(23.70%)	0.85	59.77(22.24%)	0.75	68.48(25.48%)
	RF	1	939	0.93	32.59(12.12%)	0.88	54.54(20.29%)	0.77	65.66(24.43%)

selected three band texture ratios were chosen for creating a predictive map showing forest AGB over the entire study area (see Fig. 7).

3.7. Frequency analysis

Fig. 6, 7 shows a summary of the frequently occurring bands and texture measures using all the texture models (i.e. raw texture bands, two and three band texture combinations).

Results in Fig. 6a shows that texture parameters computed from band 4 (NIR band) and band 2 (green band) contain the majority of forest AGB information. The window size that dominated the texture models was the 3 × 3 window size followed by the 7 × 7 window size (Fig. 6b). In addition, Fig. 6c shows that the co-occurrence of texture measures was predominantly selected for model development compared to the occurrence texture measures. Table 10 shows the selected variables for all the pan-sharpened image texture models (i.e. raw

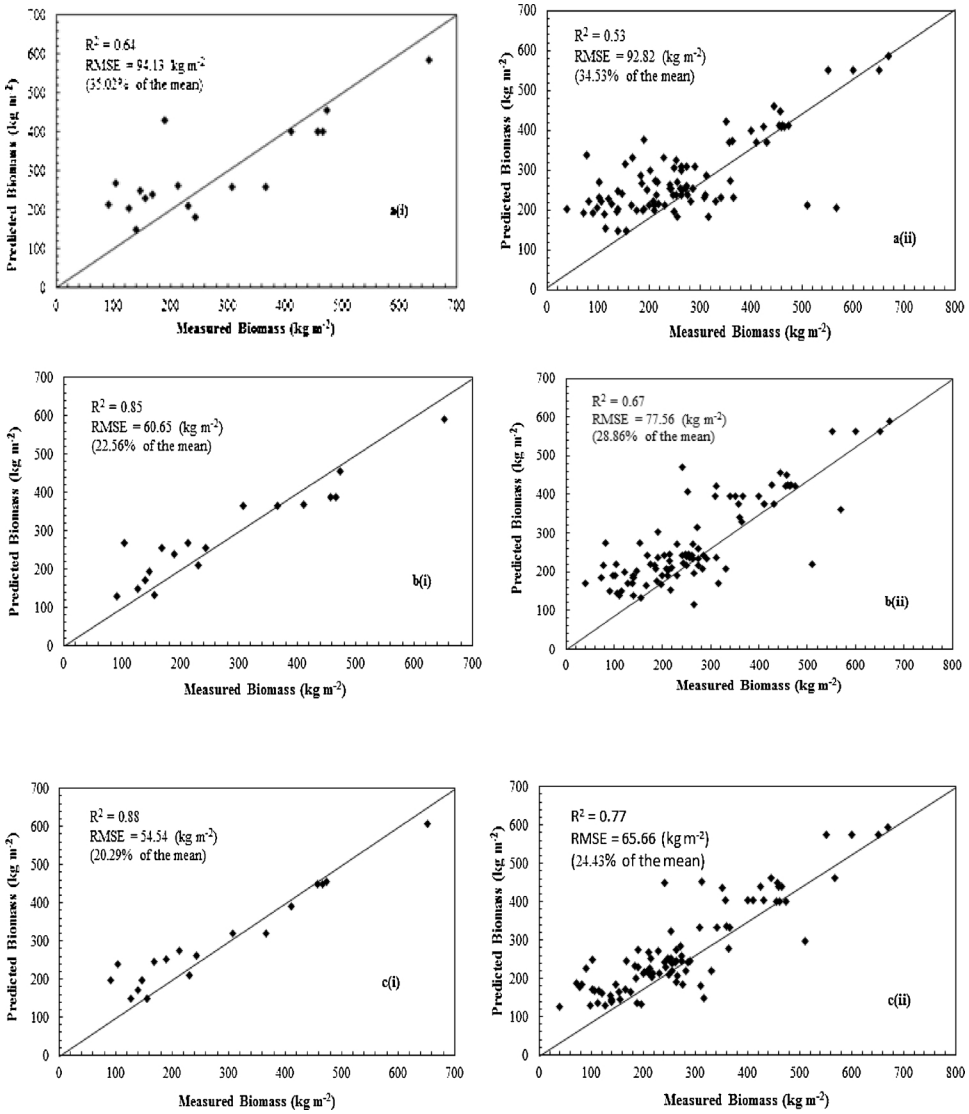

Fig. 5. Shows that the three texture band models produced the overall highest predicted performance with a R^2 of 0.88 compared to both the two texture band ratios (R^2 = 0.85) and raw band texture (R^2 = 64) based on test dataset of the pan-sharpened image. Herein a, b, and c represent the raw texture bands, two band texture and three band texture combinations, respectively and i and ii represent test dataset and cross-validation dataset, respectively.

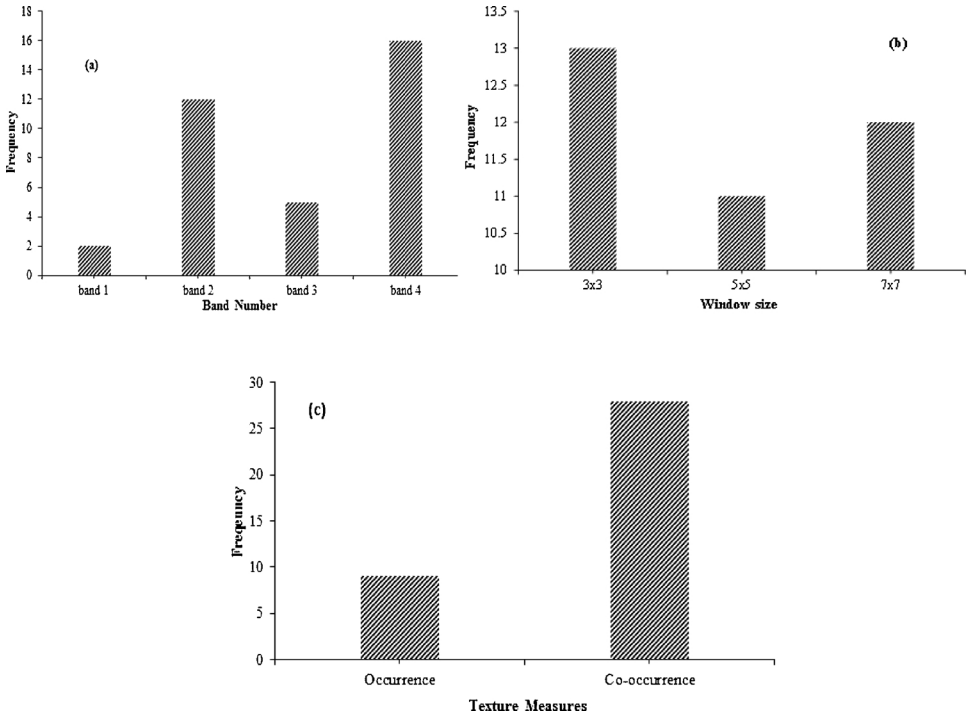

Fig. 6. Presents the frequencies of a. SPOT6 bands, b. window size, and c. texture measure in the selected models of single texture bands, 2 texture band ratios and 3 texture band ratios for the pan-sharpened image.

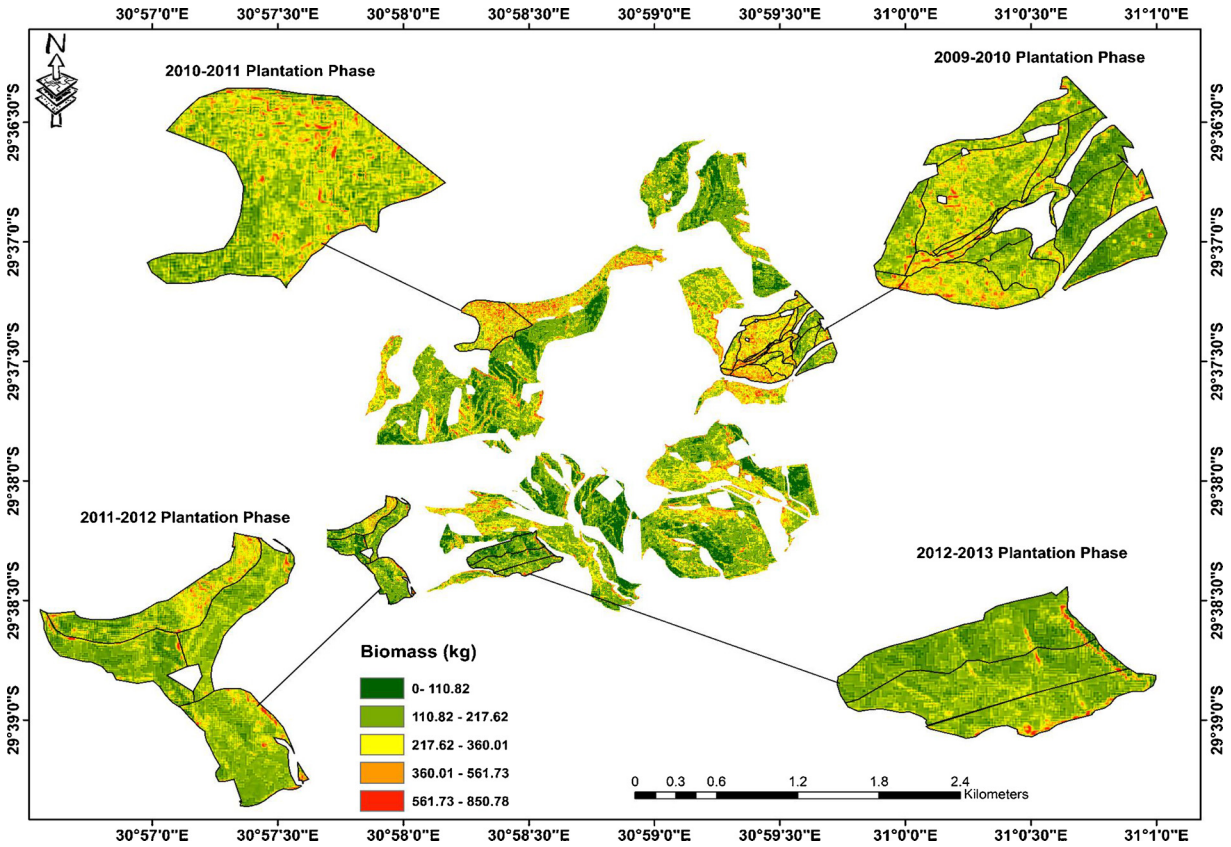

Fig. 7. Above ground biomass map derived from the best performing three texture band combinations computed from the pan-sharpened image for the 2009–2013 plantation period.

texture bands, two and three texture band ratios).

The variables were selected using the RF ensemble that selects the optimum number of variables based on the lowest average RMSE after running the backward feature elimination process repeatedly a 1000 times. Through the RF selection process, six variables were selected for raw texture bands, five variables were selected for two band texture

Table 10
Variables that were selected for constructing texture models using forward selection in multiple linear regression.

Raw bands	Two band texture ratio	Three band texture ratio
SM_C_3_B2	$MN\_C\_3\_B4 - MN\_C\_5\_B2$	$\frac{MN\_C\_3\_B4}{CR\_C\_7\_B2 \times MN\_O\_5\_B2}$
CN_C_5_B4	$MN\_C\_3\_B4 - MN\_O\_5\_B2$	$\frac{MN\_C\_3\_B4}{MN\_O\_5\_B2 \times CR\_C\_7\_B2}$
MN_C_3_B4	$MN\_O\_5\_B4 / CR\_C\_7\_B3$	$\frac{MN\_C\_3\_B4}{HM\_C\_7\_B2 \times MN\_C\_3\_B3}$
EN_O_5_B1	$MN\_C\_5\_B2 - MN\_C\_3\_B4$	$\frac{MN\_C\_3\_B4}{MN\_C\_3\_B3 \times HM\_C\_7\_B2}$
MN_C_7_B4	$MN\_C\_5\_B2 - MN\_O\_3\_B4$	$\frac{MN\_O\_5\_B4}{MN\_C\_3\_B3 \times HM\_C\_7\_B2}$
EN_C_7_B4		$\frac{MN\_C\_3\_B4}{MN\_O\_5\_B1 \times CR\_C\_7\_B3}$
CN_C_7_B4		$\frac{EN\_O\_7\_B3}{CR\_C\_7\_B3 \times HM\_C\_7\_B4}$
DR_O_5_B4		

B1, B2, B3, B4: Band 1, Band 2, Band 3 and Band 4; HM: Homogeneity, EN: Entropy, SM, Second moment, MN: Mean, DR: Data range, CR: Correlation, VR: Variance; O: Occurrence, C: Co-occurrence; 3, 5, 7: 3 × 3, 5 × 5, 7 × 7.

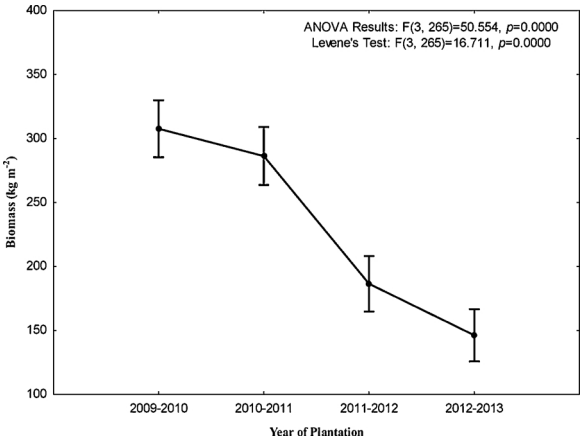

Fig. 8. Mean AGB for the five year successional dates from 2009 to 2013 computed from the predicted above-ground biomass map shown in Fig. 8.

combinations and eight variables were selected for the three band texture combination model.

Fig. 7 shows the map of AGB produced in Python language using the three band texture combinations computed from the Spot6 pan-sharpened image that yielded the highest accuracy $R^2 = 0.88$, RMSE = 54.54 (20.29%) based on an independent test dataset. Furthermore, the map also shows that lower forest AGB values are located on younger tree plantations i.e. 2011–2012 and 2012–2013. Fig. 8 shows the average forest AGB in kg m^{-2} for five years from 2009 to 2013 computed from the predicted map of biomass in Fig. 7. The results in Fig. 8 indicates that there is a significant successive variation in AGB with the highest mean AGB (325.83 kg m^{-2}) occurring in the 2009–2010 succession. Furthermore, the youngest succession 2012–2013 exhibited the lowest mean AGB (146.78 kg m^{-2}).

We conducted ANOVA statistics to assess the significance of the mean differences among the successional dates. The ANOVA results indicated that forest AGB varies significantly among the successional periods with F (3, 265) = 50.554, and p = 0.0000 and the Levene's test of homogeneity of variance revealed that data did not meet the homogeneity of variance as a result Games Howell post hoc analysis was conducted. The Games Howell post hoc analysis revealed that the significant variation in mean forest AGB was observed in successional periods that are at least two years apart. For example, trees planted in the 2009–2010 succession contained significantly high AGB compared to trees planted in 2011–2012 and 2012–2013 with p-values of 0,001,713 and 0,000010, respectively. Furthermore, trees planted in 2010–2011 contained significantly higher mean forest AGB compared to trees planted in 2011–2012 and 2012–2013 with p-values of 0,008628, and 0,000099, respectively.

4. Discussion

To establish a model for estimating forest AGB, we tested the performance of three image processing techniques (i.e. raw texture bands, two band texture combinations and three band texture combinations). The use of texture combinations in this study proved that texture parameters are capable of estimating tree biomass more adequately when compared to raw texture bands. Multivariate analysis results for the three image processing techniques showed that single texture bands produced the lowest overall accuracy ($R^2 = 0.64$ and RMSE = 94.13 kg m^{-2}) followed by some improvements using the two band texture combination ($R^2 = 0.85$ and RMSE = 60.65 kg m^{-2}). However, the highest overall accuracy was obtained using three band texture combination ($R^2 = 0.88$ and RMSE = 54.54 kg m^{-2}).

The high performance of texture measures in predicting forest AGB was anticipated, because previous research has reported significantly higher correlations between forest AGB and texture parameters (Dengsheng Lu and Batistella, 2005; Eckert, 2012). Our results showed that co-occurrence texture parameters appeared frequently in the models, thus indicating that they contained the majority of forest AGB information. These results are similar to other studies that have shown that co-occurrence texture measures contain the highest vegetation information compared to occurrence texture measures (Yuan et al., 1991; Franklin et al., 2000; Lottering and Mutanga, 2012). Comparatively, our results yielded reasonable accuracies, considering the fact that we used freely available SPOT-6 imagery as opposed to using high-resolution satellite images that are expensive. In this study higher accuracies were obtained using texture band combinations, computed from two and three texture bands.

These results coincide with the findings of Sarker and Nichol (2011), who achieved a 12% increase in model performance using simple ratio computed from 2 texture bands of AVNIR image ($R^2 = 0.88$), compared to single texture band models ($R^2 = 0.76$) for estimating forest AGB. Using Landsat-8, Dube and Mutanga (2015b), also found a high performance of texture band ratios ($R^2 = 0.53$) compared to raw texture bands ($R^2 = 0.51$) in predicting AGB of various forest plantation species. Of interest in this study, were significant improvements obtained from the three band texture combinations, which have not been previously reported in forest AGB estimations.

The high performance of the three band texture combinations can be attributed to 1) combining texture analysis with 2) band ratios and 3) the high spatial resolution of the pan-sharpened image. Texture parameters yielded good results due to their capability to simplify the tree canopy structure into homogenous pixels, by measuring the spatial distribution of image tone within a moving window using statistics (Wulder et al., 1998). We observed that our study area contained a high variation of canopy structure that resulted from a mixture of old trees with dense canopy structure and young trees with sparse canopy structure. According to Bastin et al. (2014), the canopy structure contributes to variation in grey-tone levels dense canopy structures produce coarse variation in grey-tone levels whereas sparse canopy structures produce fine variations of grey-tones. This makes texture best suited for estimating forest AGB in this study as opposed to using band ratios computed from spectral reflectance, that lack the capability of simplifying complex canopy structures. Moreover, the use of three-band texture ratios improved the accuracy of forest AGB estimation by further enhancing the capability of band ratios, to minimise errors associated with sun illumination and topographic variations on upwelling radiance (Mather and Koch, 2011; Nichol and Sarker, 2011; Dube and Mutanga, 2015b). Therefore, the combination of the three band ratio technique with texture analysis produced a model that is able to simplify complex canopy structures and thoroughly reduce topographic

and sun illumination errors on upwelling radiance.

We also believe that the high performance of the three band texture combination is as a result of the integration of optimum window size selection and the high spatial resolution of the pan-sharpened image. This is due to the fact that image texture contains information about the 'spatial' distribution of tonal variations within a band (Haralick et al., 1973), and image tone variation is directly proportional to the resolution of the pixels (Lottering and Mutanga, 2012). Therefore, selecting the optimum window sizes for forest AGB estimation increased the capability of texture models to detect and predict variation in forest AGB. These results are further affirmed by Lottering and Mutanga (2016) who found that selecting optimum spatial resolution for predicting *Gonipterus scutellatus* defoliation levels yielded higher accuracies compared to the normal spatial resolution of the Worldview-2 pan-sharpened image. Findings in this study emphasise the positive relationship between image texture and spatial resolution of an image.

Regardless of the high performance of the three texture band combinations in predicting forest AGB, we noted that accuracies achieved in this study were not higher than previously reported studies that used band texture combinations. For example, in this study, the highest accuracy obtained using three texture band combinations was $R^2 = 0.88$ and in Sarker and Nichol (2011) they obtained R^2 as high as 0.88 using a simple ratio (two band texture combinations) of texture parameters computed from ALOS AVNIR-2 image. We argue that results obtained in this study were reasonably high considering the complexity of the vegetation structure, composition and health conditions in our study area. Based on results obtained in this study, the presence of young trees planted in 2011–2013 affected the performance of the models. The results illustrated in Fig. 5 shows that AGB of old trees planted in 2009–2011 yielded higher correlations with texture parameters $R^2 = 0.70$ compared to AGB prediction of young trees $R^2 = 0.25$. These results are explained better by Bingham and Sawyer (1992), who suggested that young trees have less dense canopy structure compared to old trees, therefore the discrete variation of grey-tone for individual young trees is not easily distinguishable, because more than one tree canopy occupies a single pixel. As a result, young trees contribute to wide variation in grey-tone that cannot be accurately measured using texture parameters, which explain why their forest AGB predictions were lower than old trees.

In addition, we observed that the trees were planted within senescing sugarcane and certain areas were characterised by high tree mortality rate. The presence of senescing vegetation could have affected the spatial distribution of grey tones, as a result inhibiting the formation of distinct forest textural patterns. This would mean that areas that contain high forest AGB with dead sugarcane would be poorly estimated by texture measures. Evidence of the presence of senescing vegetation in this study was verified by the results obtained in Fig. 7, showing that the NIR band (band 4) followed by the green band (band 2) appeared most frequently on the overall texture models investigated. The high sensitivity of the green waveband to forest AGB is indicative of the presence of senescing vegetation with high chlorophyll concentration variability. These results coincides with those of Carter (1993); Gitelson et al. (1996) and Daughtry et al. (2000), who found the high sensitivity of the green waveband to chlorophyll content of senescing vegetation using spectral reflectance of hyperspectral sensors.

Furthermore, frequency analysis for optimal window size in our study indicated that the 3 × 3 window size was the most suitable for predicting AGB, followed by 7 × 7 window size. These results indicate that variability of AGB was best captured at higher resolution (smaller window size) where vegetation was less heterogeneous. We attribute these results to the high heterogeneity of the natural forest stand, consisting of shrubs such as *Chromolaena ordata* and tall grasses that could have affected the spatial distribution of grey tone of pixels in close proximity. These results are in concordance with those of Dye et al. (2012), who was able to map *Pinus patula* forest species better using variance texture measures computed from 3 × 3 window sizes. Findings from Dye et al. (2012), suggests that small window sizes contain detailed textural information of individual trees, whereas large window sizes contain texture information of the entire forest stands.

In summary, results of this study proved that the SPOT-6 pan-sharpened image is able to estimate forest AGB on the basis that effective image processing techniques are utilised. The utility of texture parameters in this study yielded promising results, however, outstanding results were achieved using three band texture combinations. Findings from this study show that the three band texture combination technique offers new opportunities for improving estimation of forest AGB, in areas with limited availability of very high spatial and spectral resolution imagery, such as worldview-2 and hyperspectral sensors, and in areas with highly complex vegetation composition and stand structure. Based on our findings, other studies should use the 3 × 3, 5 × 5 and 7 × 7 window size for mapping forest AGB, however, they should test different texture combinations to suit their particular studies. Moreover, the results obtained in this study provided insight to the invaluable contribution of the Buffelsdraai reforestation program on above-ground biomass accumulation. The results indicated that forest AGB increases with the year of succession, thus illustrating that reforestation has a high potential to meet the objectives of maximising terrestrial carbon storage through forest AGB.

5. Conclusion

This study builds from previous research studies looking at estimation of forest AGB using image texture, however a new approach was introduced using three band texture combinations. This study has shown that the SPOT-6 pan-sharpened image is capable of predicting AGB in trees planted at various plantation phases using texture combinations. Furthermore, the study revealed that:

- The SPOT-6 pan-sharpened image was able to predict AGB of older trees planted in 2010–2011 better than younger trees planted in 2011–2013.
- The green band was highly sensitive to AGB variation, thus indicating the presence of senescing vegetation.
- The three band texture combination techniques yielded higher overall accuracy in predicting forest AGB, offering new opportunities for mapping forest AGB.

This new image processing technique has not been tested by researchers and therefore provides a new perspective and approach to mapping forest AGB in complex vegetation structure. In addition, we suggest that future studies should explore this invaluable technique of optimum window selection for texture computation, to enhance the detection and prediction of geographic entities. Overall, the study proved that there are significant benefits of reforestation, especially over a long term period as forest AGB was proven to increase over time.

Acknowledgments

This research was funded by the Durban Municipality via the Durban Research Action Partnership with the University of KwaZulu-Natal. The authors would like to thank the South African Space Agency for accepting our request and providing us with such a high quality image with no charge. The authors would also like to thank Professor Mathieu Roget from the department of Land Use Planning and Management for his guidance and assistance during data collection for this research.

References

Anderson, G.L., Hanson, J.D., Haas, R.H., 1993. Evaluating landsat thematic mapper derived vegetation indices for estimating above-ground biomass on semiarid rangelands. Remote Sens. Environ. 45 (2), 165–175. https://doi.org/10.1016/0034-

4257(93)90040-5.
Barbosa, J.M., Melendez-Pastor, I., Navarro-Pedreño, J., Bitencourt, M.D., 2014. Remotely sensed biomass over steep slopes: an evaluation among successional stands of the Atlantic Forest, Brazil. Isprs J. Photogramm. Remote. Sens. 88, 91–100. https://doi.org/10.1016/j.isprsjprs.2013.11.019.
Bastin, J.-F., Barbier, N., Couteron, P., Adams, B., Shapiro, A., Bogaert, J., De Cannière, C., 2014. Aboveground biomass mapping of African forest mosaics using canopy texture analysis: toward a regional approach. Ecol. Appl. 24 (8), 1984–2001. https://doi.org/10.1890/13-1574.1.
Bingham, B.B., Sawyer, J.O., 1992. Canopy structure and tree condition of young, mature, and old-growth Douglas-fir/hardwood forests. In: Harris, R.R., Erman, D.E. (Eds.), Proceedings of the Symposium on Biodiversity of Northwestern California (Vol. Report No. 29). CA: University of California, Santa Rosa, CA. Berkeley, pp. 141–149.
Breiman, L., 2001. Random forests. Mach. Learn. 45 (1), 5–32. https://doi.org/10.1023/a:1010933404324.
Carter, G.A., 1993. Responses of leaf spectral reflectance to plant stress. Am. J. Bot. 239–243.
Castillo-Santiago, M.A., Ricker, M., de Jong, B.H.J., 2010. Estimation of tropical forest structure from SPOT-5 satellite images. Int. J. Remote Sens. 31 (10), 2767–2782. https://doi.org/10.1080/01431160903095460.
Chave, J., Andalo, C., Brown, S., Cairns, M.A., Chambers, J.Q., Eamus, D., Yamakura, T., 2005. Tree allometry and improved estimation of carbon stocks and balance in tropical forests. Oecologia 145 (1), 87–99. https://doi.org/10.1007/s00442-005-0100-x.
Daughtry, C.S.T., Walthall, C.L., Kim, M.S., de Colstoun, E.B., McMurtrey Iii, J.E., 2000. Estimating corn leaf chlorophyll concentration from leaf and canopy reflectance. Remote Sens. Environ. 74 (2), 229–239. https://doi.org/10.1016/S0034-4257(00)00113-9.
Dube, T., Mutanga, O., 2015a. Evaluating the utility of the medium-spatial resolution Landsat 8 multispectral sensor in quantifying aboveground biomass in uMgeni catchment, South Africa. Isprs J. Photogramm. Remote. Sens. 101, 36–46.
Dube, T., Mutanga, O., 2015b. Investigating the robustness of the new Landsat-8 Operational Land Imager derived texture metrics in estimating plantation forest aboveground biomass in resource constrained areas. Isprs J. Photogramm. Remote. Sens. 108, 12–32. https://doi.org/10.1016/j.isprsjprs.2015.06.002.
Dube, T., Mutanga, O., Elhadi, A., Ismail, R., 2014. Intra-and-Inter Species Biomass Prediction in a Plantation Forest: Testing the Utility of High Spatial Resolution Spaceborne Multispectral RapidEye Sensor and Advanced Machine Learning Algorithms. Sensors 14 (8), 15348.
Dye, M., Mutanga, O., Ismail, R., 2012. Combining spectral and textural remote sensing variables using random forests: predicting the age of Pinus patula forests in KwaZulu-Natal, South Africa. J. Spat. Sci. 57 (2), 193–211. https://doi.org/10.1080/14498596.2012.733620.
Eckert, S., 2012. Improved forest biomass and carbon estimations using texture measures from WorldView-2 satellite data. Remote Sens. (Basel) 4 (4), 810–829.
Franklin, S.E., Waring, R.H., McCreight, R.W., Cohen, W.B., Fiorella, M., 1995. Aerial and satellite sensor detection and classification of western spruce budworm defoliation in a subalpine forest. Can. J. Remote. Sens. 21 (3), 299–308. https://doi.org/10.1080/07038992.1995.10874624.
Franklin, S.E., Hall, R.J., Moskal, L.M., Maudie, A.J., Lavigne, M.B., 2000. Incorporating texture into classification of forest species composition from airborne multispectral images. Int. J. Remote Sens. 21 (1), 61–79. https://doi.org/10.1080/014311600210993.
Franklin, S.E., Wulder, M.A., Gerylo, G.R., 2001. Texture analysis of IKONOS panchromatic data for Douglas-fir forest age class separability in British Columbia. Int. J. Remote Sens. 22 (13), 2627–2632. https://doi.org/10.1080/01431160120769.
Gitelson, A.A., Gritz, Y., Merzlyak, M.N., 2003. Relationships between leaf chlorophyll content and spectral reflectance and algorithms for non-destructive chlorophyll assessment in higher plant leaves. J. Plant Physiol. 160 (3), 271–282. https://doi.org/10.1078/0176-1617-00887.
Gitelson, A.A., Kaufman, Y.J., Merzlyak, M.N., 1996. Use of a green channel in remote sensing of global vegetation from EOS-MODIS. Remote Sens. Environ. 58 (3), 289–298. https://doi.org/10.1016/S0034-4257(96)00072-7.
Gower, S.T., McMurtrie, R.E., Murty, D., 1996. Aboveground net primary production decline with stand age: potential causes. Trends Ecol. Evol. (Amst.) 11 (9), 378–382.
Haralick, R.M., Shanmugam, K., Dinstein, I., 1973. Textural features for image classification. IEEE Trans. Syst. Man Cybern. 610–621. https://doi.org/10.1109/TSMC.1973.4309314. SMC-3(6).
Huete, A., Didan, K., Miura, T., Rodriguez, E.P., Gao, X., Ferreira, L.G., 2002. Overview of the radiometric and biophysical performance of the MODIS vegetation indices. Remote Sens. Environ. 83 (1), 195–213. https://doi.org/10.1016/S0034-4257(02)00096-2.
Ismail, R., Mutanga, O., Kumar, L., Bob, U., 2008. Determ in ing the optimal spatial resolution of remotely sensed data for the detection of SIREX NOCTILIO infestations in p ine plantations in KWAZULU-NATAL, South Africa. South Afr. Geogr. J. 90 (1), 22–31. https://doi.org/10.1080/03736245.2008.9725308.
James, G., Witten, D., Hastie, T., Tibshirani, R., 2013. An Introduction to Statistical Learning Vol 6 Springer.
Kayitakire, F., Hamel, C., Defourny, P., 2006. Retrieving forest structure variables based on image texture analysis and IKONOS-2 imagery. Remote Sens. Environ. 102 (3–4), 390–401. https://doi.org/10.1016/j.rse.2006.02.022.
Lottering, R., Mutanga, O., 2012. Estimating the road edge effect on adjacent Eucalyptus grandis forests in KwaZulu-Natal, South Africa, using texture measures and an artificial neural network. J. Spat. Sci. 57 (2), 153–173. https://doi.org/10.1080/14498596.2012.733617.
Lottering, R., Mutanga, O., 2016. Optimising the spatial resolution of WorldView-2 pan-sharpened imagery for predicting levels of Gonipterus scutellatus defoliation in KwaZulu-Natal, South Africa. Isprs J. Photogramm. Remote. Sens. 112, 13–22. https://doi.org/10.1016/j.isprsjprs.2015.11.010.
Lu, D., 2005. Aboveground biomass estimation using Landsat TM data in the Brazilian Amazon. Int. J. Remote Sens. 26 (12), 2509–2525. https://doi.org/10.1080/01431160500142145.
Lu, D., Batistella, M., 2005. Exploring TM image texture and its relationships with biomass estimation in Rondônia, Brazilian Amazon. Acta Amazon. 35 (2), 249–257.
Lu, D., Mausel, P., Brondizio, E., Moran, E., 2002. Above-Ground biomass estimation of successional and mature forests using TM images in the amazon Basin. In: Richardson, D.E., van Oosterom, P. (Eds.), Advances in Spatial Data Handling: 10th International Symposium on Spatial Data Handling. Springer Berlin Heidelberg, Berlin, Heidelberg, pp. 183–196.
Lu, D., Batistella, M., Moran, E., 2005. Satellite estimation of aboveground biomass and impacts of forest stand structure. Photogramm. Eng. Remote Sensing 71 (8), 967–974.
Marceau, D.J., Gratton, D.J., Fournier, R.A., Fortin, J.-P., 1994. Remote sensing and the measurement of geographical entities in a forested environment. 2. The optimal spatial resolution. Remote Sens. Environ. 49 (2), 105–117. https://doi.org/10.1016/0034-4257(94)90047-7.
Materka, A., Strzelecki, M., 1998. Texture Analysis Methods–a Review. Technical university of lodz, institute of electronics, COST B11 report, Brussels, pp. 9–11.
Mather, P.M., Koch, M., 2011. Computer Processing of Remotely-sensed Images : an Introduction. Wiley-Blackwell, Chichester, West Sussex, UK; Hoboken, NJ.
Moskal, L.M., Franklin, S.E., 2001. Classifying multilayer forest structure and composition using high resolution, compact airborne spectrographic imager image texture. Paper Presented at the ASPRS Proceedings.
Mucina, L., Rutherford, M.C., 2006. The Vegetation of South Africa, Lesotho and Swaziland. South African National Biodiversity Institute, Pretoria.
Mutanga, O., Skidmore, A.K., 2004. Integrating imaging spectroscopy and neural networks to map grass quality in the Kruger National Park, South Africa. Remote Sens. Environ. 90 (1), 104–115. https://doi.org/10.1016/j.rse.2003.12.004.
Mutanga, O., Adam, E., Cho, M.A., 2012. High density biomass estimation for wetland vegetation using WorldView-2 imagery and random forest regression algorithm. Int. J. Appl. Earth Obs. Geoinf. 18, 399–406.
Nichol, J.E., Sarker, M.L.R., 2011. Improved biomass estimation using the texture parameters of two high-resolution optical sensors. Geosci. Remote Sens. IEEE Trans. 49 (3), 930–948. https://doi.org/10.1109/TGRS.2010.2068574.
Nowak, D.J., Crane, D.E., 2002. Carbon storage and sequestration by urban trees in the USA. Environ. Pollut. 116 (3), 381–389. https://doi.org/10.1016/S0269-7491(01)00214-7.
Pan, Y., Birdsey, R.A., Fang, J., Houghton, R., Kauppi, P.E., Kurz, W.A., Canadell, J.G., 2011. A large and persistent carbon sink in the world's forests. Science 333 (6045), 988–993.
Peerbhay, K., Mutanga, O., Lottering, R., Ismail, R., 2016. Mapping Solanum mauritianum plant invasions using WorldView-2 imagery and unsupervised random forests. Remote Sens. Environ. 182, 39–48. https://doi.org/10.1016/j.rse.2016.04.025.
Rubner, Y., Puzicha, J., Tomasi, C., Buhmann, J.M., 2001. Empirical evaluation of dissimilarity measures for color and texture. Comput. Vis. Image Underst. 84 (1), 25–43. https://doi.org/10.1006/cviu.2001.0934.
Sarker, L.R., Nichol, J.E., 2011. Improved forest biomass estimates using ALOS AVNIR-2 texture indices. Remote Sens. Environ. 115 (4), 968–977. https://doi.org/10.1016/j.rse.2010.11.010.
Sousa, A.M.O., Gonçalves, A.C., Mesquita, P., Marques da Silva, J.R., 2015. Biomass estimation with high resolution satellite images: a case study of Quercus rotundifolia. Isprs J. Photogramm. Remote. Sens. 101, 69–79. https://doi.org/10.1016/j.isprsjprs.2014.12.004.
St-Louis, V., Pidgeon, A.M., Radeloff, V.C., Hawbaker, T.J., Clayton, M.K., 2006. High-resolution image texture as a predictor of bird species richness. Remote Sens. Environ. 105 (4), 299–312. https://doi.org/10.1016/j.rse.2006.07.003.
Strait, M., Rahmani, S., Merkurev, D., 2008. Evaluation of Pan-sharpening Methods. UCLA Department of Mathematics, Los Angeles, USA.
Tuttle, E.M., Jensen, R.R., Formica, V.A., Gonser, R.A., 2006. Using remote sensing image texture to study habitat use patterns: a case study using the polymorphic white-throated sparrow (Zonotrichia albicollis). Glob. Ecol. Biogeogr. 15 (4), 349–357. https://doi.org/10.1111/j.1466-822X.2006.00232.x.
Verrelst, J., Rivera, J.P., Veroustraete, F., Muñoz-Marí, J., Clevers, J.G.P.W., Camps-Valls, G., Moreno, J., 2015. Experimental Sentinel-2 LAI estimation using parametric, non-parametric and physical retrieval methods – a comparison. Isprs J. Photogramm. Remote. Sens. 108, 260–272. https://doi.org/10.1016/j.isprsjprs.2015.04.013.
Wang, W., Yao, X., Yao, X., Tian, Y., Liu, X., Ni, J., Zhu, Y., 2012. Estimating leaf nitrogen concentration with three-band vegetation indices in rice and wheat. Field Crops Res. 129, 90–98. https://doi.org/10.1016/j.fcr.2012.01.014.
Wulder, M.A., LeDrew, E.F., Franklin, S.E., Lavigne, M.B., 1998. Aerial image texture information in the estimation of northern deciduous and mixed wood forest leaf area index (LAI). Remote Sens. Environ. 64 (1), 64–76. https://doi.org/10.1016/S0034-4257(97)00169-7.
Yuan, X., King, D., Vlcek, J., 1991. Sugar maple decline assessment based on spectral and textural analysis of multispectral aerial videography. Remote Sens. Environ. 37 (1), 47–54. https://doi.org/10.1016/0034-4257(91)90049-C.